JOURNAL OF AIRCRAFT
Vol. 35, No. 2, March–April 1998

Ice Accretion Prediction on Multielement Airfoils

Giuseppe Mingione* and Vincenzo Brandi†
Italian Aerospace Research Center (CIRA), Capua, 81043 Italy

The aim of this paper is to present the Italian icing computational environment code, I²CE, developed by CIRA, and discuss its evaluation for ice accretion on single and multielement airfoils. The aerodynamic module of the code is based on a potential panel method, whereas the thermodynamic module is based on the classic Messinger model. Different ways to solve the time-dependent ice accretion problem have been taken into account. A comparison between theoretical calculations using multi-time-step, single-time-step, or predictor–corrector procedures and experimental data has been carried out. The effect of the flowfield viscosity on droplet trajectories and the influence of different approaches for the convective heat exchange coefficient calculation have been considered. The influence on the impingement of the actual droplet size distribution has been taken into account and a comparison with a standard median volumetric diameter calculation is presented.

Nomenclature

C = chord
C_f = skin friction coefficient
c_D = droplet drag coefficient
c_p = constant pressure specific heat
d = droplet diameter
F = fraction of nonfreezing water
g = gravity acceleration
h = convective heat transfer coefficient
K_s = standard sand grain roughness
k = thermal conductivity
M = Mach number
m = droplet mass
N = number of droplet size intervals in a natural spectrum
Nu = Nusselt number
P = pressure
Pr = Prandtl number
Re = Reynolds number
S, S_w = droplet cross section and wetted area
St_K = dimensionless roughness parameter
s = curvilinear abscissa from lower trailing edge
$srist$ = stagnation point curvilinear abscissa
T = temperature
$\dot{T}_d$ = droplet temperature time derivative
t = accretion time
U = velocity
$\ddot{x}$, $\ddot{y}$, $\ddot{z}$ = droplet acceleration Cartesian component
α = incidence
β = droplet collection efficiency
γ_i = ith coordinate direction angle
θ = boundary-layer momentum thickness
ν = cinematic viscosity
ρ = density

Subscripts

a = air variable
c = variable referred to chord
d = droplet variable
e = external to the boundary-layer variable
i = ice variable
j = referred to a droplet size interval in a natural spectrum
k = variable referred to roughness
r = relative variable
w = water variable
wa = wall variable
x, y, z = along x, y, z direction
0 = stagnation variable
∞ = freestream variable

Presented as Paper 97-0177 at the AIAA 35th Aerospace Sciences Meeting, Reno, NV, Jan. 6–10, 1997; received April 27, 1997; revision received Sept. 10, 1997; accepted for publication Nov. 15, 1997.

*Research Engineer, Aerodynamic and Propulsion Department, Transport Aircraft Aerodynamics Group, Via Maiorise. E-mail: g.mingione@cira.it.

†Research Engineer, Aerodynamic and Propulsion Department, Transport Aircraft Aerodynamics Group, Via Maiorise. E-mail: v.brandi@cira.it. Member AIAA.

I. Introduction

In the past few years there have been increasing efforts in the area of icing research and, particularly, in the numerical simulation of ice accretion phenomenon. Several codes were developed for two- and three-dimensional applications by ONERA,[1] the Defence Research Agency (DRA),[2] NASA,[3] the Boeing Commercial Airplane Group,[4] and École Polytechnique de Montréale.[5] All of the codes still employ the classical Messinger model[6] to evaluate ice accumulation, although some limitations are known, particularly when the air temperature approaches the freezing point.[7] A code developed by the Italian Aerospace Research Center (CIRA) to evaluate the ice accretion on single and multielement airfoils is described in this paper and the results of some applications are presented.

II. Code Structure

Ice accretion on aircraft components is a time-dependent phenomenon that can take place when an aircraft flies in clouds at subfreezing temperature. In these conditions, down to −40°C, water droplets can be supercooled, i.e., they are in a liquid but not stable state: once they strike an object like a wing leading edge, they can immediately freeze or run back downstream and freeze on the wing surface.

Three steps are needed to perform ice accretion simulation: 1) aerodynamic calculation of the velocity field around the body; 2) calculation of the water droplet trajectories to evaluate the amount of water that impinges on the body, i.e., the collection efficiency; and 3) calculation of the body surface heat transfer coefficient and ice accretion calculation.

There are two different procedures with which to address the accretion-time problem. In the first one, the overall accre-

tion time is divided into steps, and for each time step the ice accretion is evaluated. The second one consists of performing a predictor–corrector-type calculation. The aerodynamic flowfield on the clean airfoil is calculated, and the droplet trajectories and ice accumulated are computed during the total accretion time as a single time step (predictor phase). The collection efficiency estimated in the predictor phase does not take into account that the airfoil, because of the ice accumulation, changes its shape and, consequently, affects the collection efficiency during the accretion time. To attempt to reproduce the collection efficiency time history, the aerodynamic flowfield and droplet trajectories are recalculated on this first estimated ice shape, obtaining a new set of impingement data. The final ice shape (corrector phase) is calculated by dividing the total accretion time into steps and, for each time step, using the collection efficiency data obtained by means of a linear time interpolation between the values evaluated on the clean airfoil and those computed on the first estimated iced airfoil. The present code can perform the ice accretion with both procedures.

A. Aerodynamic and Droplet Trajectories Module

The aerodynamic flowfield has been evaluated by using a panel method, whereas the droplet trajectories are obtained by adopting a Lagrangian approach. The coupling between the droplet trajectories and the aerodynamic flowfield is considered weak, which means that the aerodynamic field is computed and then kept frozen for the successive computation of the droplet trajectories. Thus, no interaction of the droplet motion on the aerodynamic field is accounted for. The main forces acting on a small spherical droplet moving in a steady airflow are its aerodynamic drag and weight: the effect of buoyancy forces is to be negligible. The droplet temperature is calculated through an energy balance. Therefore, the following equations are solved:

$$\begin{aligned} m\ddot{x} &= \tfrac{1}{2}\rho_a U_r^2 S c_D \cos\gamma_x \\ m\ddot{y} &= \tfrac{1}{2}\rho_a U_r^2 S c_D \cos\gamma_y \\ m\ddot{z} &= \tfrac{1}{2}\rho_a U_r^2 S c_D \cos\gamma_z + mg \\ mc_{\mathrm{pw}}\dot{T}_d &= h(T - T_d)S_w \end{aligned} \tag{1}$$

The drag coefficient c_D is assumed as a function of the Reynolds number based on the relative velocity U_r and the droplet diameter. The expressions adopted for the evaluation of the function $c_D(Re_d)$ are obtained from experimental data.[8]

B. Thermodynamic Module

Initially, the convective heat transfer coefficient is calculated by using an integral boundary-layer calculation method. The criterion to evaluate the transition from laminar to turbulent flow is based on the Reynolds number, $Re_k = U_e K_s/\nu$, calculated through K_s and U_e.

When Re_k is lower than 6×10^2, the boundary layer is assumed to be laminar and h can be evaluated through the Spalding analogy[9]:

$$h = \frac{0.293 k U_e^{1.435}}{\sqrt{\nu \int_0^s U_e^{1.87}\,\mathrm{d}s}} \tag{2}$$

For the turbulent boundary layer ($Re_k \geq 6 \times 10^2$), the momentum thickness is computed, extending the Thwaites' method to turbulent velocity profiles[9]:

$$\theta = \frac{0.0263\nu^{0.2}}{U_e^{3.4}}\left(\int_{s_{\mathrm{tr}}}^s U_e^4\,\mathrm{d}s\right)^{0.8} + \theta_{\mathrm{tr}} \tag{3}$$

where θ_{tr} is the momentum thickness at transition location.

C_f is calculated through the Makkonen semiempirical correlation[10] as a function of θ and K_s, according to the following relation:

$$\frac{C_f}{2} = \frac{0.168}{\{\ell n[846(\theta/K_s)]\}^2} \tag{4}$$

Finally, the convective heat transfer coefficient is estimated as

$$h = \rho_a c_p U_e \frac{C_f/2}{Pr + (1/St_K)\sqrt{C_f/2}} \tag{5}$$

where St_K is

$$St_K = 0.52\left(\frac{u_\tau K_s}{\nu}\right)^{-0.45} Pr^{0.8} \tag{6}$$

with

$$u_\tau = \sqrt{0.0125 U_e^2 (\theta U_e/\nu)^{-0.25}} \tag{7}$$

Once h is calculated, the classical Messinger model is employed to evaluate the ice shape. In this model, water droplets that impinge on a panel either freeze immediately at the point of impact or run back along the airfoil surface into the next downstream panel, i.e., it is assumed that there is a thin, continuous film of water covering the surface or ice. A mass and energy balance is performed in each control volume (panel) to compute F and T_{wa}.

The following mass flow contributions are taken into account on the ith panel: 1) water incoming from the previous panel, which is a known quantity from the balance performed on the $(i-1)$th panel; 2) the impinging water, which depends upon the collection efficiency; 3) the evaporation/sublimation mass rate; 4) the solidified water; and 5) the water running back to the next panel.

Once F and T_{wa} are computed through the energy balance, the water running back to the next panel can be evaluated from the mass balance, because it is the last unknown factor of the problem.

The energy balance is performed with the following heat flow contribution: 1) convective cooling, 2) sublimation/evaporation energy, 3) freezing and heating or cooling of impinging water, 4) freezing and heating or cooling of run-back water, 5) kinetic energy of incoming water, and 6) heat flux from anti-icing device.

The energy balance depends on F and T_{wa} in an implicit manner. An iterative procedure is used to solve the energy balance for F and T_{wa} by assuming an initial guess for T_{wa} and drawing F; if F is consistent with the wall temperature, i.e., $T_{\mathrm{wa}} = 0 \rightarrow 0 \leq F \leq 1$, the calculation is stopped; otherwise the wall temperature is updated and the calculation is repeated. Further details on the mass and energy balance contributions can be found in Ref. 11.

Table 1 Geometric and aerodynamic conditions for NACA 0012 test case

Variable	Value
C	0.5334 m
U_∞	67.05 m/s
P	101,300 Pa
LWC	1 g/m^3
t	360 s
α	4 deg
MVD	20 μm
Droplet distribution	Monodispersed
K_s	0.001
ρ_i	910 kg/m^3

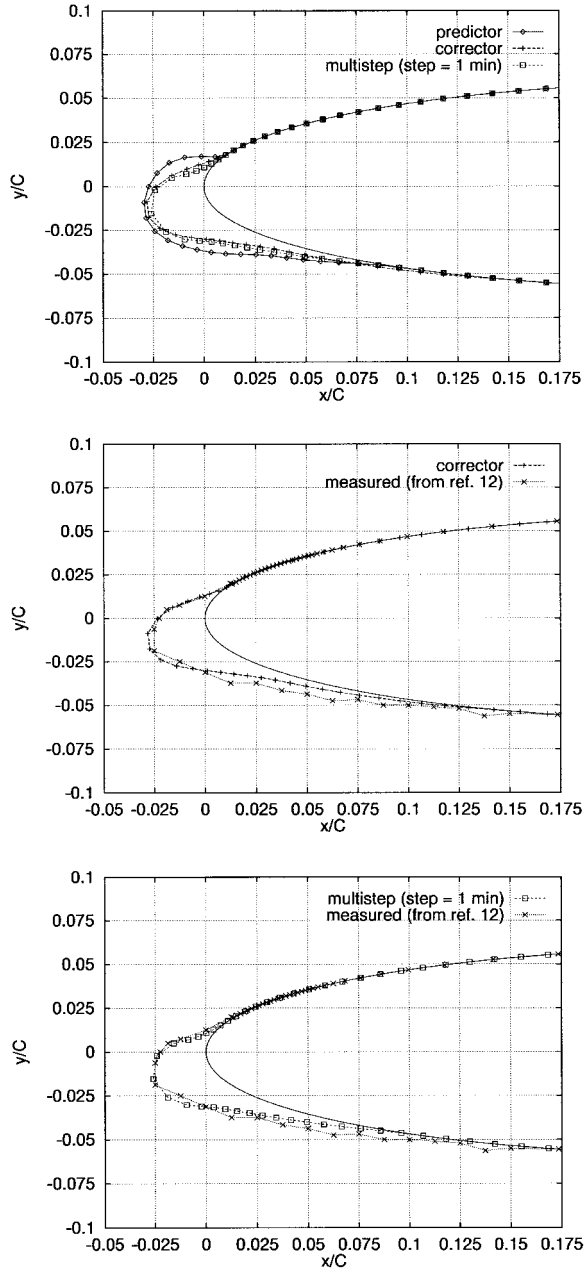

Fig. 1 NACA 0012 airfoil, $T_0 = -15°F$, $T_\infty = -19°F$ ($-28.4°C$).

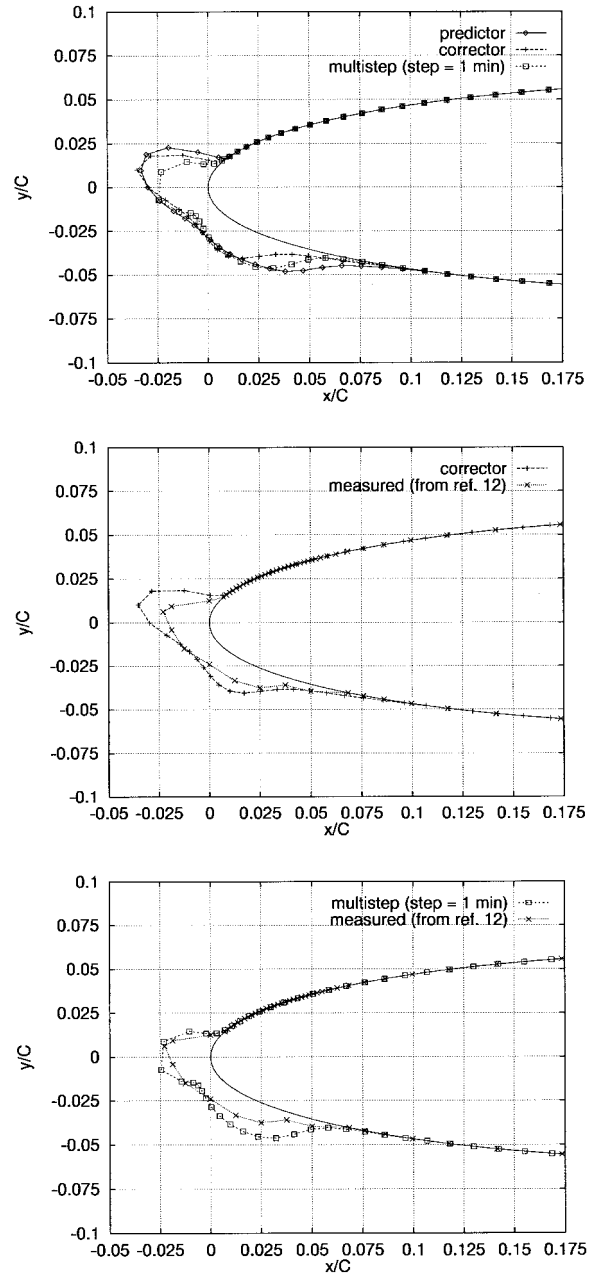

Fig. 2 NACA 0012 airfoil, $T_0 = 18°F$, $T_\infty = 14°F$ ($-10°C$).

III. Accretion Time-Procedure Comparison

Although all of the existing codes make use of similar methodologies, they adopt different approaches to evaluate the aerodynamic flowfield. The French code (CAPTA) solves the full potential equations, whereas the NASA code (LEWICE) and the Canadian one (CANICE-ME) make use of a panel method, but all of them employ the Messinger model to evaluate the ice accumulation. Nevertheless, there are some differences in dealing with the accretion time. The NASA code employs a multi-time-step procedure, whereas the French code uses a predictor–corrector approach. Finally, because the trajectory calculation may be a quite onerous task, particularly for multielement airfoils, some codes often use a single-time-step procedure. There is no doubt that a reduction of the number of time steps involves a remarkable computing-time reduction. Some experimental ice accretion shapes[12] at different temperatures have been compared with the ones predicted by the present code. The geometric and aerodynamic data in Table 1 refer to a NACA 0012 airfoil.

The calculations have been carried out with a predictor–corrector technique as well as a step-by-step strategy.

At the lowest air temperatures, $T_\infty = -19°F$ ($-28.4°C$), the typical rime ice shape takes place; these physical conditions are well simulated by the CIRA ice accretion model, so that the agreement between the calculated ice shapes and the measured ones is very good and there are not appreciable differences between the predictor–corrector and the step-by-step results (Fig. 1).

Raising the air temperature, the behavior of ice accretion leaves the rime ice conditions and approaches the glaze one. The comparison between the measured and theoretical ice shapes for $T_\infty = 14°F$ ($-10°C$) (Fig. 2) is adequate, but the agreement is more favorable when the multi-time-step procedure is employed. When $T_\infty = 24°F$ ($-4.5°C$), the theoretical result still agrees well with the experimental shapes (Fig. 3). In all of the test cases, except the rime one (Fig. 1), the predictor approach also provides fairly good results.

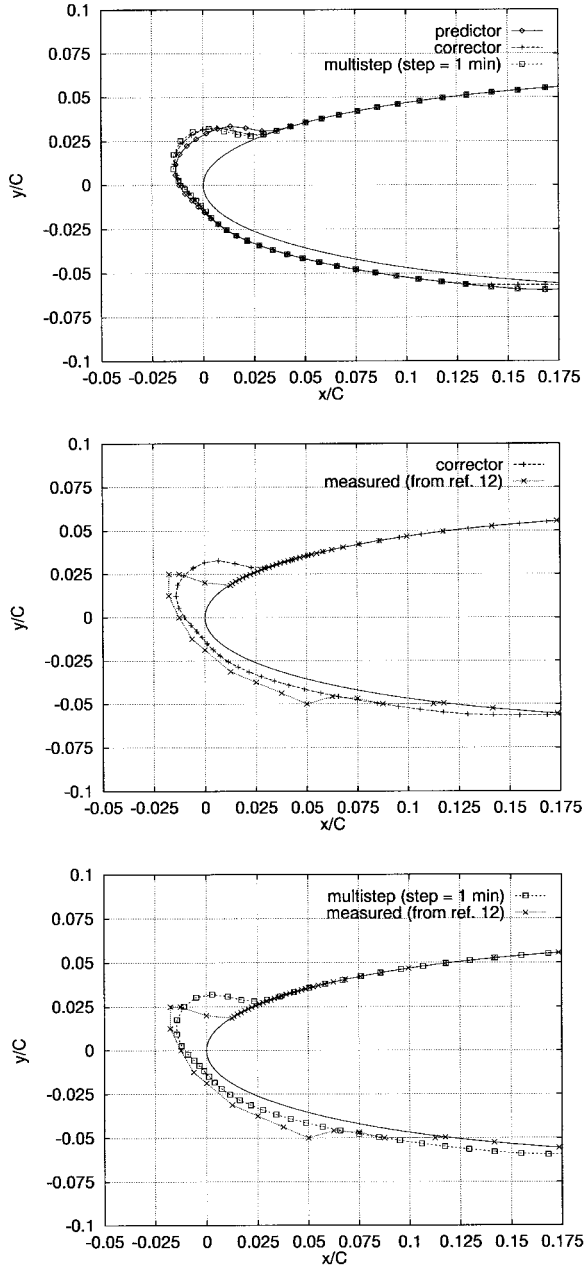

Fig. 3 NACA 0012 airfoil, T_0 = 28°F, T_∞ = 24°F (−4.5°C).

IV. Viscous/Nonviscous Ice Accretion Calculation

An ice accretion calculation was performed on a two-component airfoil at two different angles of attack to evaluate the influence of the air viscosity on the droplet trajectories. At first, the aerodynamic flowfield was evaluated with a panel method (without viscosity effect); later, to account for the viscosity effect, the aerodynamic flowfield was evaluated by means of the MAVIAN (multi-element airfoil viscous-inviscid interactive analysis) code, developed at CIRA, in which a potential flow solver is coupled to an integral boundary-layer calculation method. Both direct and inverse formulation have been carried out.[13] Trajectory and ice accretion calculations were performed for both the viscous and the inviscid cases. The geometric and aerodynamic conditions in Table 2 have been taken into account.

In Figs. 4–6, the calculation results are shown for α = 0 and 8.1 deg. There is an influence both at low and at high incidence, but in the former, the effect is more evident on the rear body (Fig. 6a), while in the latter it is more obvious on the main body (Fig. 5b). This behavior can be explained because

Table 2 Geometric and aerodynamic conditions for two-component airfoil ice accretion

Variable	Value
α	0 and 8.1 deg
Re	2,660,000
C	0.57 m
U_∞	59.36 m/s
T_∞	258.15 K
M	0.185
P	101,300 Pa
LWC	1 g/m^3
t	360 s
MVD	20 μm
Droplet distribution	Monodispersed
K_s	0.001
ρ_i	910 kg/m^3

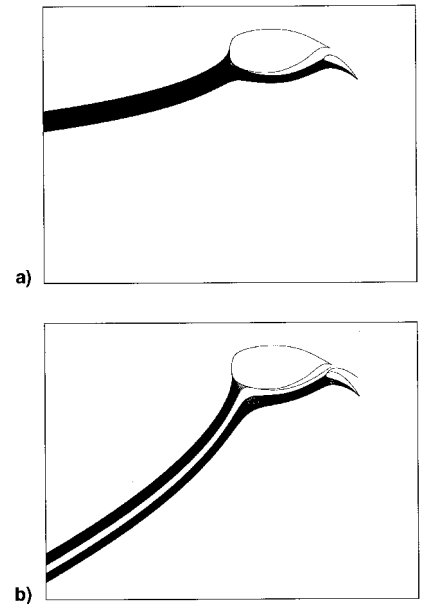

Fig. 4 Droplet trajectories on a two-component airfoil. α = a) 0 and b) 8.1 deg.

at low incidence, although the viscous effects are negligible, the trajectories impinging on the rear body are quite close to the main body (Fig. 4a), so that the collection efficiency on the rear body is affected more by the viscosity than that on the main body. At α = 8.1 deg, on the other hand, the trajectories impinging on the rear body pass far away from the main component (Fig. 4b) but, because the incidence is larger, the viscosity effects on the collection efficiency are more obvious.

Because of the lack of experimental ice accretion shapes on multicomponent configurations, CIRA theoretical results have only been compared with other existing numerical simulations.[14]

V. Convective Heat Transfer Coefficient Evaluation: A Comparison Among Different Methods

Because the convective heat transfer contribution in the energy balance is the most dominant term, there is no doubt that a suitable prediction of this term involves a better evaluation of ice accretion on the airfoil.

The coefficient h, for a turbulent boundary layer, is a function of C_f. An analysis has been performed to evaluate how the transition location and the particular method employed to calculate the skin friction coefficient affect the convective heat transfer coefficient and, consequently, the ice accretion.

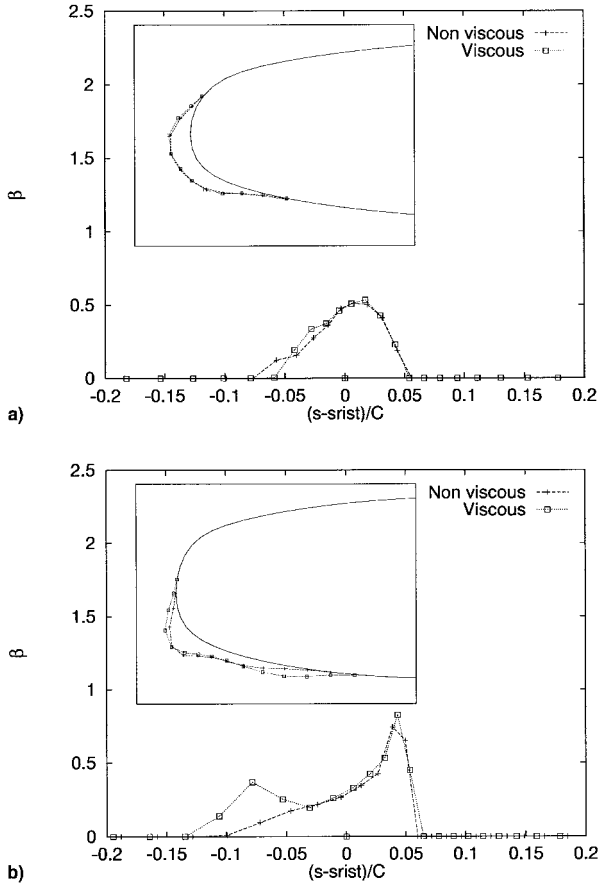

Fig. 5 Two-component airfoil: collection efficiency on the main body. α = a) 0 and b) 8.1 deg.

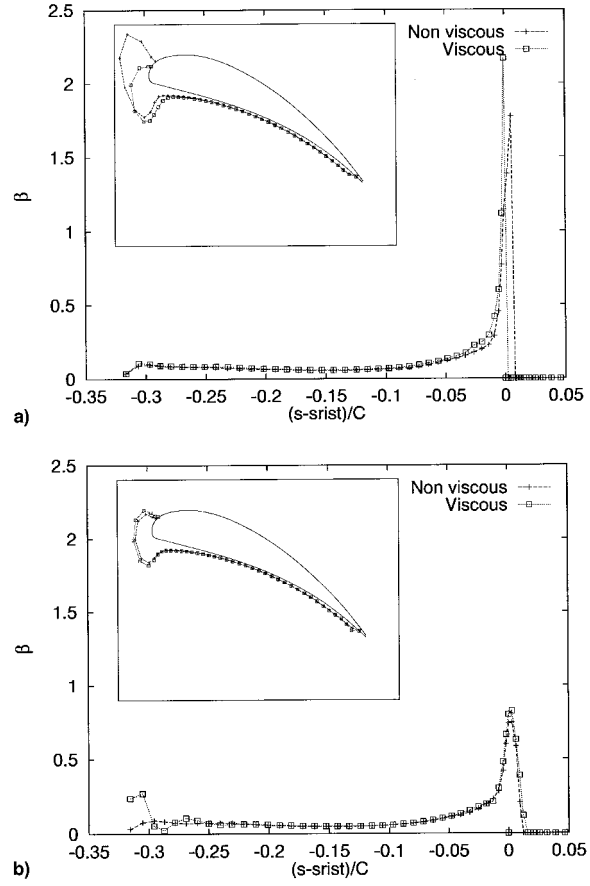

Fig. 6 Two-component airfoil: collection efficiency on the rear body. α = a) 0 and b) 8.1 deg.

Three methods have been taken into account to compute the boundary-layer quantities: 1) the integral method currently incorporated in the standard version of the icing code, 2) a finite difference method with the Cebeci–Smith turbulence model,[9] and 3) a finite difference method with the κ-ω turbulence model.[15]

The last two methods were incorporated in the icing code by means of the calculation of C_f, whereas h was computed with Eq. (5). The calculation was carried out on the NACA 0012 airfoil with the geometric and aerodynamic conditions in Table 3.

A first set of calculations was performed by holding the transition point fixed. The κ-ω model was used to predict the transition onset; then the calculation was repeated with the Cebeci–Smith model and the integral method by fixing the transition at the same location predicted by the κ-ω model.

The convective heat transfer coefficient and the corresponding ice accretion are shown in Fig. 7a; the integral method and the finite difference method with the Cebeci–Smith turbulence model provide results that agree quite well, whereas the κ-ω model predicts a larger convective heat transfer coefficient. Ice accretion follows the same trend: the larger convective heat transfer coefficient involves a greater ice thickness.

The transition location influence was estimated. The integral method was employed with the standard $Re_k \geq 600$ criterion to predict the transition point location. Then the result was compared with what was previously obtained at the fixed transition location (Fig. 7b). Using the $Re_k \geq 600$ criterion, the transition from laminar to turbulent flow is anticipated and located in the stagnation region, which involves a larger ice thickness in this area.

Because it was difficult to judge which of the theoretical predictions was more correct, a comparison with available convective heat transfer flight test data on the NACA 0012 airfoil (chord = 0.5334 m, T_∞ = 273.15 K) was carried out.[16] To perform a suitable comparison with the experimental data, h was expressed in the Frossling number form ($Nu/\sqrt{Re_c}$) for two different airfoil roughness patterns (Fig. 8); K_s employed in the calculation was estimated as a function of the roughness concentration and shape.[17] The theoretical convective heat transfer coefficient was computed with the integral boundary-layer calculation method with the assumption that the transition starts at s/C = 0.025, where the Frossling number flight test data show sudden growth; this growth is more obvious for the densely roughened airfoil (Fig. 8b), but, for both the roughened patterns, it is not clear if it is caused by a real transition onset or by a local roughness effect.

The data in the laminar part agree very well, whereas in the turbulent part the Frossling number is overestimated by the theoretical data. This behavior could be a consequence of the difficulties in simulating the actual roughness elements with the standard roughness parameter required in the ice accretion theoretical model or because of the lack of a more gradual transition from the laminar to turbulent flow in our theoretical model.

VI. Droplet Spectrum Effect

The existence of dangerous icing conditions caused by large water droplets ($d \geq 200$ μm) has been demonstrated.[18] In these particular conditions, the aerodynamic performance degradation caused by the ice accretion can be remarkable and not directly related to the calculated median volumetric diameter (MVD), because this parameter does not adequately characterize the larger drops but is thought to be caused by the larger drops measured in the distribution. To understand the influence on the ice accretion phenomenon of larger droplets in an actual droplet distribution, an icing event encountered by the Beech-

Table 3 Geometric and aerodynamic conditions for NACA 0012 airfoil convective heat transfer calculation comparison

Variable	Value
α	4 deg
Re	2,772,000
C	0.5334 m
U_∞	67.05 m/s
T_∞	268.7 K
M	0.204
P	101,300 Pa
LWC	1 g/m^3
t	360 s
MVD	20 μm
Droplet distribution	Monodispersed
K_s	0.001
ρ_i	910 kg/m^3

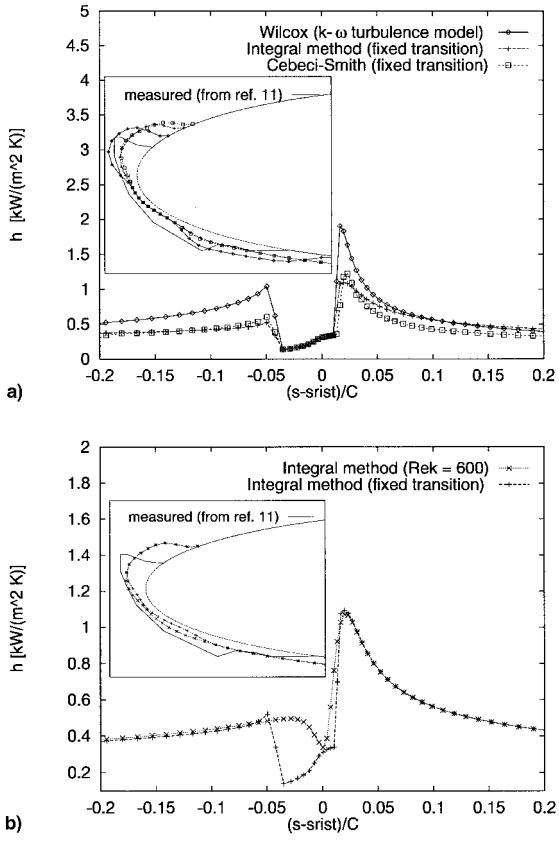

Fig. 7 Convective heat transfer coefficient and the following ice accretion on a NACA 0012 airfoil: a) comparison among three boundary-layer methods and b) transition location effect.

craft Super King research aircraft has been taken into account.[19]

This event was characterized by MVD and liquid water content (LWC) values that caused a remarkable performance degradation to help an aircraft derouting. The same MVD and LWC values were encountered by aircraft in the past and were faced without any trouble. The difference between the two icing events was ascribed to the presence of larger droplets in the natural droplet spectrum (Fig. 9a). Figure 9a shows data from FSSP, 1D-C, and 2D-C devices, which are spectrometer and optical probes to measure hydrometeor concentrations and sizes. An approximate histogram spectrum has been employed to reproduce the actual trend of the natural distribution; a Langmuir–Blodgett droplet size distribution (type D),[20] relative to the same MVD and LWC values, has also been superimposed to the actual spectrum. An ice accretion calcula-

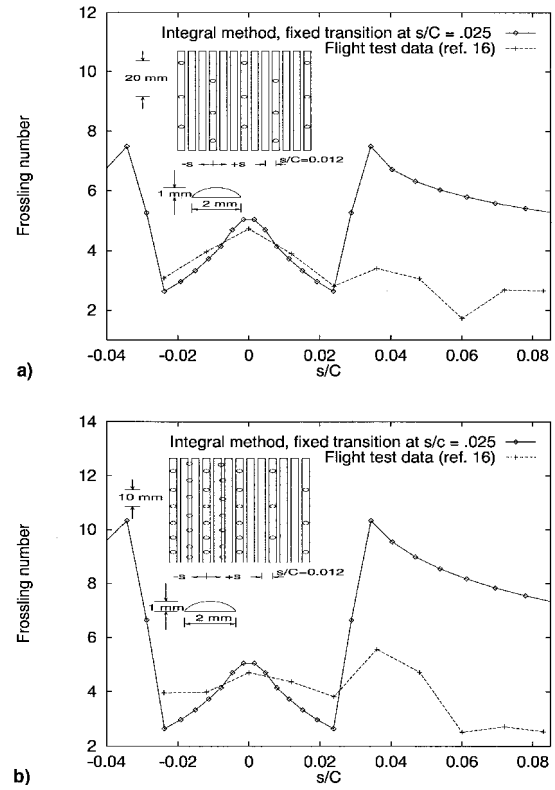

Fig. 8 Frossling number comparison on a NACA 0012, α = 0 deg (Re_c = 2,007,527, M = 0.150): a) sparsely roughened airfoil, K_s = 0.00056, and b) densely roughened airfoil, K_s = 0.0028.

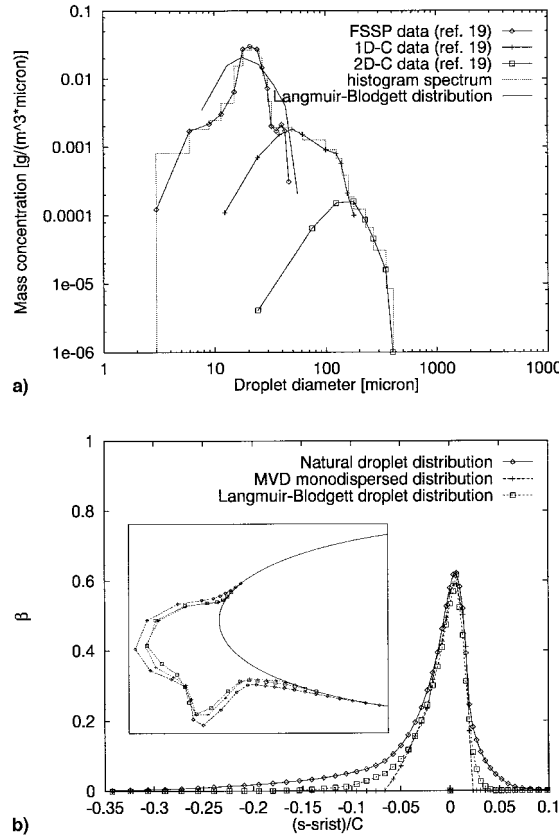

Fig. 9 Super King aircraft icing event on February 26, 1982, MVD = 25 μm, LWC = 0.5 g/m^3: a) actual and assumed droplet diameter distribution and b) impingement and ice accretion comparison on a NACA 0012.

Table 4 Conditions for NACA 0012 airfoil droplet spectrum effects evaluation

Variable	Value
α	4 deg
C	1.83 m
U_∞	89.4 m/s
T_∞	263.7 K
P	57,150 Pa
LWC	0.5 g/m^3
t	90 min
MVD	25 μm
K_s	0.001
ρ_i	910 kg/m^3

tion was carried out with the histogram droplet distribution, the Langmuir–Blodgett distribution, and the monodispersed MVD value. For each droplet size interval of the histogram spectrum, the collection efficiency was evaluated as if it were a monodispersed distribution with a diameter equal to the midpoint of the droplet size interval, e.g., in Fig. 9a, $d_j = 4.5$ μm for droplets with diameters from 3 to 6 μm; finally, the collection efficiency was computed by averaging the collection efficiency calculated for every droplet size interval with the LWC value related to the same interval, i.e.,

$$\beta(s) = \sum_{j=1}^{N} \beta_j(s) \frac{\mathrm{LWC}_j}{\mathrm{LWC}} \tag{8}$$

Because data on Super King airfoil and flight test conditions during the icing event were not available, the calculations were carried out on a NACA 0012 at the conditions shown in Table 4.

The impingement and the ice accretion comparison are shown in Fig. 9b. While the monodispersed MVD and Langmuir–Blodgett droplet distribution ice shapes are comparable, a larger ice thickness and impingement area with higher aerodynamic performance penalties characterize the case with the natural droplet distribution.

VII. Conclusions

A code developed at CIRA for the ice accretion evaluation on single- and multi-element airfoils was presented along with validation test cases and particular applications. The following conclusions can be drawn:

1) The predictor–corrector time-accretion procedure can be considered satisfactory; in fact, in all tested cases, excluding $T_\infty = -14$°F (-10°C), there was only a slight difference between the ice shapes calculated with this technique and the most rigorous step-by-step procedure.

2) It is fundamental to adopt the actual droplet distribution to study some peculiar icing conditions.

3) Viscous effects on trajectory calculation may be meaningful in particular conditions.

4) The integral method for the evaluation of the convective heat transfer coefficient provides satisfactory results (comparable with those obtained by the more sophisticated κ-ω turbulence model); an important role is played by the transition onset prediction.

References

[1]Hedde, T., and Guffond, D., "Improvement of the ONERA 3-d Icing Code, Comparison with 3D Experimental Shapes," AIAA Paper 93-0169, Jan. 1993.

[2]Gent, R. W., "TRAJICE2—A Combined Water Droplet and Ice Accretion Prediction Code for Airfoils," Royal Aerospace Establishment, TR 90054, May 1990.

[3]Wright, W. B., "Users Manual for the Improved NASA Lewis Ice Accretion Code LEWICE 1.6," NASA CR 198355, June 1995.

[4]Bidwell, C. S., and Mohler, S. R., "Trajectory and Ice Accretion Calculations for a Swept NACA 0012 Wing, a Swept MS-317 Wing, an Axisymetric Inlet, and a Boeing 737-200 Inlet," AIAA Paper 95-0755, Jan. 1995.

[5]Brahimi, M. T., Tran, P., Paraschivoiu, I., and Tezok, F., "Prediction of Ice Accretion on Supercritical and Multi-Element Airfoils," AIAA Paper 95-0754, Jan. 1995.

[6]Messinger, B. L., "Equilibrium Temperature of an Unheated Icing Surface as Function of Airspeed," *Journal of the Aeronautical Sciences*, Vol. 20, No. 1, 1953, pp. 29–42.

[7]Olsen, M., and Walker, E., "Experimental Evidence for Modifying the Current Physical Model for the Ice Accretion on Aircraft Surfaces," NASA TM 87184, May 1986.

[8]Vicini, A., and Mingione, G., "Computation of Three-Dimensional Droplet Trajectories and Temperature for the C.I.R.A. Icing Wind Tunnel," Italian Aerospace Research Center, CIRA-TN-95-0052, March 1995.

[9]Cebeci, T., and Bradshaw, P., *Physical and Computational Aspects of Convective Heat Transfer*, Springer–Verlag, New York, 1988, pp. 94, 95, 184–201.

[10]Kays, W. M., and Crawford, M. E., *Convective Heat Transfer*, McGraw–Hill, New York, 1980, p. 420.

[11]Mingione, G., and Brandi, V., "A Code for the Evaluation of Ice Accretion on Multi-Element Airfoils," Italian Aerospace Research Center, CIRA-TN-96-089, July 1996.

[12]Shin, J., and Bond, T., "Results of an Icing Test on a NACA 0012 Airfoil in the NASA Lewis Icing Research Tunnel," AIAA Paper 92-0647, Jan. 1992.

[13]Quagliarella, D., "Aerodynamic Analysis of a Flapped Airfoil Configuration for the YAK-130S Airplane," Italian Aerospace Research Center, CIRA-TN-97-038, June 1997.

[14]Tran, P., Brahimi, M. T., Tezok, F., and Paraschivoiu, I., "Numerical Simulation of Ice Accretion on Multiple Element Configurations," AIAA Paper 96-0869, Jan. 1996.

[15]Wilcox, D. C., "Simulation of Transition with a Two-Equation Turbulence Model," *AIAA Journal*, Vol. 32, No. 2, 1994, pp. 247–255.

[16]Newton, J. E., Van Fossen, G. J., Poinsatte, P. E., and DeWitt, K. J., "Measurement of Local Convective Heat Transfer Coefficients from a Smooth and Roughened NACA 0012 Airfoil: Flight Test Data," AIAA Paper 88-0287, Jan. 1988.

[17]Cebeci, T., "The Calculation of Flow over Iced Airfoils," AIAA Paper 88-0112, Jan. 1988.

[18]Cooper, W. A., Sand, W. R., Politovich, M. K., and Veal, D. L., "Effects of Icing on Performance of a Research Airplane," *Journal of Aircraft*, Vol. 21, No. 9, 1984, pp. 708–715.

[19]Ashenden, R., and Marwitz, J. D., "Supercooled Large Droplet Distributions in the Natural Environment and Comparison to Artificial Drizzle from Air Force Water Spray-Tanker," *Proceedings of the FAA International Conference on Inflight Aircraft Icing* (Springfield, VA), DOT/FAA/AR-96/8, II, 1996, pp. 33–43.

[20]Heinrich, A., Ross, R., Zumwalt, G., Provorse, J., Padmanabhan, V., Thompson, J., and Riley, J., *Aircraft Icing Handbook*, Vol. 1, DOT/FAA/CT-88/8-1, March 1991, pp. 1–13.